J|A|C|S ARTICLES

Published on Web 06/04/2010

Thorpe−Ingold Acceleration of Oxirane Formation Is Mostly a Solvent Effect

Jakub Kostal and William L. Jorgensen*

Department of Chemistry, Yale University, 225 Prospect Street, New Haven, Connecticut 06520-8107

Received March 21, 2010; E-mail: william.jorgensen@yale.edu

Abstract: The Thorpe−Ingold hypothesis for the *gem*-dimethyl effect in the cyclization reactions of 2-chloroethoxide derivatives has been investigated computationally in the gas phase and in aqueous solution. Ab initio MP2/6-311+G(d,p) and CBS-Q calculations reveal little intrinsic difference in reactivity with increasing α-methylation for the series of reactants **1**−**3**. However, inclusion of continuum hydration or of explicit hydration through mixed quantum and statistical mechanics (MC/FEP) simulations does reproduce the substantial, experimentally observed rate increases with increasing α-methylation. Analysis of the MC/FEP results provides clear evidence that the rate increases stem primarily from increased steric hindrance to hydration of the nucleophilic oxygen atom with increasing α-methylation. Thus, the *gem*-dimethyl acceleration of oxirane formation for **1**−**3** is found to be predominantly a solvent effect.

Introduction

Most intramolecular reactions proceed faster than their intermolecular analogues owing to the more favorable entropy change on passing to the transition state.[1] In the formation of five- or six-membered rings, such entropic effects contribute to rate enhancements. On the other hand, in the case of formation of three- and four-membered rings, increased ring strain may be offsetting and retard cyclization. However, to overcome the unfavorable enthalpic conditions, one can take advantage of an accelerated rate of cyclization resulting from addition of alkyl substituents positioned on the acyclic carbon backbone tethering the two reacting termini.[2] Specifically, the *gem*-dialkyl effect has been studied extensively since its discovery by Beesley, Thorpe, and Ingold in 1915.[3−5] The original explanation hypothesized that substitution of alkyl groups for hydrogens on a methylene carbon leads to a sterically induced reduction of the internal angle of the carbon chain, which brings the reacting centers closer together.[3] This compression was experimentally confirmed by X-ray measurements and was argued to be sufficient to account for the rate variations.[6,7] A classic example is provided by the chlorohydrins **1**−**3**, which undergo cyclization with relative rates of 1:21:252.[8,9]

During the past century, the *gem*-dialkyl effect has been widely used in synthetic organic chemistry to improve the outcome of cyclizations. Early examples involved the acyloin and dinitrile condensations of substituted polymethylene compounds, where the shorter distances between the reacting groups resulting from methyl substitutions were argued to be roughly proportional to the reaction yields.[10] The effect has subsequently been examined for numerous reactions, including Diels−Alder cycloadditions, ene reactions, Claisen rearrangements, electrophilic cyclizations, radical cyclizations, transition-metal-catalyzed cyclizations, and ring-closing metathesis of acyclic dienes.[8]

In addition to the Thorpe−Ingold explanation, other hypotheses have emerged focusing on medium and larger ring formations.[11−14] Shifts in conformer populations upon methylation can help favor ring formation, and the significance of the small change in bond angles, ca. 3°, upon *gem*-methylation has been questioned.[13] For small ring formation, Bach and Dmitrenko reported that *gem*-dimethyl substitution lowers the strain energy of cyclopropanes, cyclobutanes, epoxides, and dimethyldioxirane by 6−10 kcal/mol relative to the unsubstituted analogues.[15] However, the results are sensitive to the choice of reference systems; Bachrach's recent computations indicate that the differences in ring strain for *gem*-dimethyl-substituted cyclopropane and cyclobutane compared to the unsubstituted cycloalkanes are less than 2 kcal/mol.[16] Corresponding benefits

(1) Page, M. J.; Jencks, W. P. *Proc. Natl. Acad. Sci. U.S.A.* **1971**, *68*, 1678–1683.
(2) Kirby, A. J. *Adv. Phys. Org. Chem.* **1980**, *17*, 183–278.
(3) Beesley, R. M.; Ingold, C. K.; Thorpe, J. F. *J. Chem. Soc.* **1915**, *107*, 1080–1106.
(4) Ingold, C. K. *J. Chem. Soc.* **1921**, *119*, 305–329.
(5) Ingold, C. K.; Sako, S.; Thorpe, J. F. *J. Chem. Soc.* **1922**, *120*, 1117–1198.
(6) Derissen, J. L. *Acta Crystallogr.* **1970**, *B26*, 901–904.
(7) Kirby, A. J.; Lloyd, G. J. *J. Chem. Soc., Perkin Trans. 2* **1972**, 1753–1761.
(8) Jung, M. E.; Piizzi, G. *Chem. Rev.* **2005**, *105*, 1735–1766.
(9) Nilsson, H.; Smith, L. *Z. Phys. Chem.* **1933**, *166A*, 136–146.
(10) Dale, J. *J. Chem. Soc.* **1963**, 93–111.
(11) (a) Bruice, T. C.; Pandit, U. K. *J. Am. Chem. Soc.* **1960**, *82*, 5858–5865. (b) Bruice, T. C.; Pandit, U. K. *Proc. Natl. Acad. Sci. U.S.A.* **1960**, *46*, 402–404.
(12) Allinger, N. L.; Zalkow, V. *J. Org. Chem.* **1960**, *25*, 701–704.
(13) Schleyer, P. v. R. *J. Am. Chem. Soc.* **1961**, *83*, 1368–1378.
(14) (a) Parrill, A. L.; Dolata, D. P. *Tetrahedron Lett.* **1994**, *35*, 7319–7322. (b) Parrill, A. L.; Dolata, D. P. *J. Mol. Struct.* **1996**, *370*, 187–202.
(15) (a) Bach, R. D.; Dmitrenko, O. *J. Org. Chem.* **2002**, *67*, 2588–2599. (b) Bach, R. D.; Dmitrenko, O. *J. Org. Chem.* **2002**, *67*, 3884–3896.
(16) Bachrach, S. M. *J. Org. Chem.* **2008**, *73*, 2466–2468.

10.1021/ja1023755

Scheme 1. S_N2 Cyclization Reaction of 2-Chloroethanol Analogues

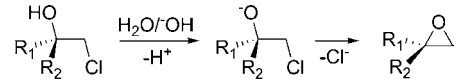

1: R_1, R_2 = H, H
2: R_1, R_2 = CH_3, H
3: R_1, R_2 = CH_3, CH_3

to related transition states are then expected to be slight, as the precursor is also stabilized by branching, as in neopentane vs pentane.[16]

Solvent effects are also known to account for striking rate variations in many organic reactions.[17] In view of our prior investigations,[18] curiosity arose concerning the reactions of **1**−**3**. A significant role of solvation in the kinetics for the cyclizations seemed possible since the rate data were obtained in protic media and in view of the steric changes near the nucleophilic oxygen. Thus, in order to separate intrinsic (gas-phase) and solvation effects, quantum and statistical mechanics calculations have been carried out at different levels of theory, employing various solvation models, on the cyclizations of chlorohydrins to form epoxides under basic conditions (Scheme 1).

Computational Details

The experimental study of the 2-chloroethanol analogues was carried out in water with sodium hydroxide as base at room temperature.[9] Thus, the present computations examined the internal S_N2 reactions of the 2-chloroethoxide analogues to yield the epoxides in both the gas phase and aqueous solution. Gas-phase structures were obtained by performing Hartee−Fock (HF)[19] and MP2 calculations,[20] using the 6-31+G(d,p) and 6-311+G(d,p) basis sets,[21−23] along with complete basis set CBS-Q compound calculations.[24] Geometries were fully optimized; all minima were verified to have no imaginary vibrational frequencies. Enthalpy and free energy barriers were evaluated at 298 K, including the changes in vibrational energy. Transition structures were initially identified with the HF method using the synchronous transit-guided quasi-Newton (STQN) approach.[25,26] The obtained geometries served as starting points for subsequent optimizations with the MP2 and CBS-Q methods. The transition structures were verified to have only one negative eigenvalue in their diagonalized force-constant matrices, and their associated eigenvectors were confirmed to correspond to motion along the reaction coordinate.

In order to estimate the influence of hydration, the self-consistent reaction-field (SCRF) continuum approach was employed using the IEF version of the polarizable continuum model (PCM)[27] in single-point calculations. The solute cavity was defined by interlocking van der Waals spheres centered at atomic positions. The reaction field was represented by the apparent surface charge (ACS) method, in which the point charges are located on the surface of the molecular cavity.[27]

Monte Carlo (MC) statistical mechanics calculations were also carried out using free energy perturbation (FEP) theory in the gas phase and in explicit water at 298 K. In this case, free energy changes are computed with statistical perturbation theory in a windowing format with double-wide sampling.[18] The reacting system was treated with the PDDG/PM3 molecular orbital method, which has been extensively tested for gas-phase structures and energetics[28−30] and has provided excellent results in solution-phase studies of S_N2 reactions,[31] nucleophilic aromatic substitution reactions,[32] decarboxylations,[33,34] and Cope eliminations.[35] The solution-phase simulations are carried out as mixed quantum and molecular mechanics (QM/MM) calculations,[17,36,37] where the solutes are treated quantum mechanically using the PDDG/PM3 method, and, for water, the solvent molecules are represented with the TIP4P model.[38] The solute−water interactions use the unscaled CM3P atomic charges[39] for the solute atoms in the Coulomb terms and the all-atom OPLS force field for the Lennard-Jones interactions.[37] The solvent boxes contained 500 water molecules, and periodic boundary conditions were used in the NPT ensemble at 298 K and 1 atm. The dimensions of the simulation cells were ca. $25 \times 25 \times 25$ Å^3. Solute−solvent and solvent−solvent intermolecular cutoff distances of 12 Å were employed for the reaction in water, based roughly on center-of-mass separations.

In the MC/FEP approach, each FEP window entailed 2.5×10^4 configurations of equilibration followed by 4.0×10^4 configurations of averaging in the gas phase and 2.5×10^6 configurations of equilibration, followed by 4.0×10^6 configurations of averaging in solution with attempted solute moves occurring every 100 configurations. Conformational equilibria of the 2-chloroethoxide analogues were examined by obtaining a potential of mean force (PMF) for perturbation of the O−C−C−Cl angle. The probabilities of sampling the *gauche* and *anti* conformations were then derived from the PMF. A novel two-dimensional PMF mapping technique was implemented to identify the transition states for the reaction

(17) Reichardt, C. *Solvents and Solvent Effects in Organic Chemistry*, 3rd ed.; Wiley-VCH: Weinheim, Germany, 2003; Chapt. 5.
(18) Acevedo, O.; Jorgensen, W. L. *Acc. Chem. Res.* **2010**, *43*, 142–151.
(19) (a) Roothaan, C. C. J. *Rev. Mod. Phys.* **1951**, *23*, 69. (b) Pople, J. A.; Nesbet, R. K. *J. Chem. Phys.* **1954**, *22*, 571–572.
(20) (a) Møller, C.; Plesset, M. S. *Phys. Rev.* **1934**, *46*, 618–622. (b) Head-Gordon, M.; Pople, J. A.; Frisch, M. J. *Chem. Phys. Lett.* **1988**, *153*, 503–506. (c) Saebø, S.; Almlöf, J. *Chem. Phys. Lett.* **1989**, *154*, 83–89. (d) Frisch, M. J.; Head-Gordon, M.; Pople, J. A. *Chem. Phys. Lett.* **1990**, *166*, 275–280. (e) Frisch, M. J.; Head-Gordon, M.; Pople, J. A. *Chem. Phys. Lett.* **1990**, *166*, 281–289. (f) Head-Gordon, M.; Head-Gordon, T. *Chem. Phys. Lett.* **1994**, *220*, 122–128.
(21) Hehre, W. J.; Ditchfield, R.; Pople, J. A. *J. Chem. Phys.* **1972**, *56*, 2257.
(22) Hariharan, P. C.; Pople, J. A. *Theor. Chem. Acta* **1973**, *28*, 213–222.
(23) Hehre, W. J.; Radom, L; Schleyer, P. v. R.; Pople, J. A. *Ab Initio Molecular Orbital Theory*; Wiley: New York, 1986; pp 86−87.
(24) (a) Nyden, M. R.; Petersson, G. A. *J. Chem. Phys.* **1981**, *75*, 1843–1862. (b) Petersson, G. A.; Bennett, A; Tensfeldt, T. G.; Al-Laham, M. A. *J. Chem. Phys.* **1988**, *89*, 2193–2218. (c) Petersson, G. A.; Al-Laham, M. A. *J. Chem. Phys.* **1991**, *94*, 6081–6090. (d) Petersson, G. A.; Tensfeldt, T.; Montgomery, J. A. *J. Chem. Phys.* **1991**, *94*, 6091–6101. (e) Montgomery, J. A.; Ochterski, J. W.; Petersson, G. A. *J. Chem. Phys.* **1994**, *101*, 5900–5909.
(25) Peng, C.; Schlegel, H. B. *Isr. J. Chem.* **1993**, *33*, 449–454.
(26) Peng, C.; Ayala, P. Y.; Schlegel, H. B.; Frisch, M. J. *J. Comput. Chem.* **1996**, *17*, 49–56.
(27) Tomasi, J.; Mennucci, B.; Cances, E. *J. Mol. Struct.* **1999**, *464*, 211–226.
(28) Repasky, M. P.; Chandrasekhar, J.; Jorgensen, W. L. *J. Comput. Chem.* **2002**, *23*, 1601–1622.
(29) Tubert-Brohman, I.; Guimarães, C. R. W.; Repasky, M. P.; Jorgensen, W. L. *J. Comput. Chem.* **2003**, *25*, 138–150.
(30) Tubert-Brohman, I.; Guimarães, C. R. W.; Jorgensen, W. L. *J. Chem. Theory Comput.* **2005**, *1*, 817–823.
(31) (a) Vayner, G.; Houk, K. N.; Jorgensen, W. L.; Brauman, J. I. *J. Am. Chem. Soc.* **2004**, *126*, 9054–9058. (b) Chen, X.; Regan, C. K.; Craig, S. L.; Krenske, E. H.; Houk, K. N.; Jorgensen, W. L.; Brauman, J. I. *J. Am. Chem. Soc.* **2009**, *131*, 16162–16170.
(32) Acevedo, O.; Jorgensen, W. L. *Org. Lett.* **2004**, *6*, 2881–2884.
(33) Acevedo, O.; Jorgensen, W. L. *J. Am. Chem. Soc.* **2005**, *127*, 8829–8834.
(34) Acevedo, O.; Jorgensen, W. L. *J. Org. Chem.* **2006**, *71*, 4896–4902.
(35) Acevedo, O.; Jorgensen, W. L. *J. Am. Chem. Soc.* **2006**, *128*, 6141–6146.
(36) (a) Warshel, A. *Acc. Chem. Res.* **2002**, *35*, 385–395. (b) Gao, J.; Ma, S.; Major, D. T.; Nam, K.; Pu, J.; Truhlar, D. G. *Chem. Rev.* **2006**, *106*, 3188–3209. (c) Senn, H. M.; Thiel, W. *Angew. Chem., Int. Ed.* **2009**, *48*, 1198–1229.
(37) Kaminski, G. A.; Jorgensen, W. L. *J. Phys. Chem. B* **1998**, *102*, 1787–1796.
(38) Jorgensen, W. L.; Chandrasekhar, J.; Madura, J. D.; Impey, W.; Klein, M. L. *J. Chem. Phys.* **1983**, *79*, 926–935.
(39) Thompson, J. D.; Cramer, C. J.; Truhlar, D. G. *J. Comput. Chem.* **2003**, *24*, 1291–1304.

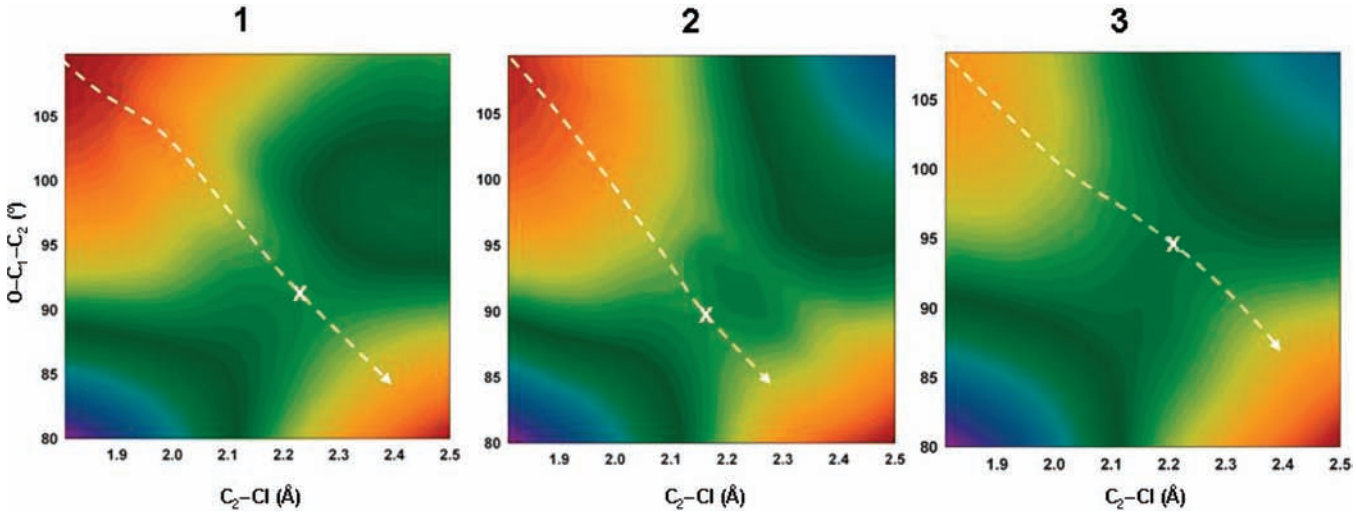

Figure 1. 2-D PMFs for the cyclization of 2-chloroethoxide analogues as depicted in Scheme 1 from PDDG-PM3/MC/FEP simulations. The "X" marks the transition structure; contour lines are spaced every 0.5 kcal/mol. The dashed lines illustrate the presumed reaction paths.

Table 1. Energies of the *Gauche* Conformers Relative to *Anti* of the 2-Chloroethoxide Analogues[a]

		HF/6-31+G(d,p)		MP2/6-31+G(d,p)		MP2/6-311+G(d,p)		CBS-Q		PDDG/PM3	
		g^+	g^-	g^+	g^-	g^+	g^-	g^+	g^-	g^+	g^-
1	ΔE	4.67		4.18		3.63		4.43		3.46	
	ΔH	4.60		4.09		3.54		4.35			
	ΔG	4.63		4.19		3.62		4.40		3.50	
2	ΔE	4.91	5.00	4.88	4.91	4.36	4.35	4.71	4.62		
	ΔH	4.89	4.94	4.86	4.86	4.35	4.32	4.69	4.55	3.05	3.71
	ΔG	4.85	5.01	4.85	4.91	4.33	4.34	4.69	4.64	2.97[b]	3.82[b]
3	ΔE	5.49		5.74		5.18		5.23		2.59	
	ΔH	5.45		5.70		5.15		5.19			
	ΔG	5.48		5.74		5.19		5.23		2.83[b]	

[a] Results in kcal/mol from gas-phase geometry optimizations. ΔE (0 K) includes the zero-point energy change. ΔH and ΔG also include the thermal corrections to 298 K. For g^+ and g^-, the C−C−C−Cl dihedral angles are ca. 180° and 60°, respectively. [b] From gas-phase FEP calculations.

in the gas phase and in solution. This technique projects the PMF calculations, simultaneously perturbing the C_2-Cl distance and the $O-C_1-C_2$ angle, onto a grid generated around a guess for the transition state in an automated, one-step process, allowing for a more accurate and computationally faster sampling of the regions of interest on the free energy surface. This approach effectively avoids sampling regions of high free energy in the far corners of the 2-D map. Ab initio gas-phase results provided an initial guess for the transition states. The range of the perturbed reaction coordinates was determined from their initial optimized values in the reactants and their final values calculated from a grid around the transition state guess, with a ±0.3 Å boundary with respect to the C_2-Cl distance and ca. ±10° with respect to the $O-C_1-C_2$ angle. Figure 1 shows the resultant free energy maps from the QM/MM simulations for **1**, **2**, and **3**. Activation barriers were subsequently evaluated by direct perturbations from the reactants to the transition states identified from the 2-D PMF scheme. Relative reaction rates were calculated from the activation energies using transition-state theory, ignoring any potential recrossing or tunneling effects. Uncertainties in the free energies reported were computed by propagating the standard deviation (σ_i) on each individual ΔG_i.[40] Unless otherwise noted, all reported free energy values from present MC/FEP simulations have a statistical error of ≤0.1 kcal/mol. BOSS 4.7[40] was used for PDDG/PM3, MM, MC, FEP, and QM/MM calculations; MOPAC 6.0[41] was also used for PDDG/PM3 optimizations; and Gaussian 03[42] was used for the ab initio calculations.

Results and Discussion

Energetics and Structure. In order to correctly estimate activation barriers for the cyclizations, free energy changes associated with conformational equilibria of the 2-chloroethoxide analogues (ΔG_{eq}) were evaluated in the gas phase and in solution (Tables 1 and 2). In Table 1, the *anti* conformers, which are the reactive rotamers for the cyclizations, are noted to be preferred in the gas phase for all analogues; the populations of the *gauche* conformations are negligible. It is reasonable that there is a significant electrostatic preference for having the formally negative oxygen atom *anti* to the electronegative chlorine; it is also consistent with favorable $n(O)-\sigma^*(CCl)$ orbital mixing. In solution, however, the relative populations of the *gauche* conformations increase and, in the case of QM/MM simulations, even slightly exceed the populations of *anti* conformations. This is likely due to a decrease in the free energies of hydration resulting from a greater polarity for the *gauche* conformations, as is well-known for 1,2-dihaloethanes.

(40) Jorgensen, W. L.; Tirado-Rives, J. *J. Comput. Chem.* **2005**, *26*, 1689–1700.
(41) Stewart, J. J. P. *MOPAC*, Version 6.0; Fujitsu Limited: Tokyo, Japan, 1999.
(42) Frisch, M. J. et al. *Gaussian 03*Revision C.02;, Gaussian, Inc.: Wallingford, CT, 2004.

Table 2. Relative Free Energies (Δ*G* in kcal/mol) of *Gauche* Conformers of the 2-Chloroethoxide Analogues (kcal/mol) in Aqueous Solution at 25 °C

	HF-PCM/6-31+G(d,p)		MP2-PCM/6-31+G(d,p)		PDDG-PM3/MC/FEP	
	g^+	g^-	g^+	g^-	g^+	g^-
1	1.21		1.36		-0.17 ± 0.29	
2	0.87	1.53	0.81	1.51	-0.47 ± 0.19	-0.68 ± 0.24
3	1.91		1.93		-1.06 ± 0.35	

Table 3. Energetic Results and Relative Rates for the Cyclization Reactions in the Gas Phase[a]

		HF/6-31+G(d,p)	MP2/6-31+G(d,p)	MP2/6-311+G(d,p)	CBS-Q	PDDG/PM3
1	$\Delta E^{\ddagger}$	4.99	5.48	7.32	3.01	
	$\Delta H^{\ddagger}$	4.93	5.40	7.27	2.89	13.00
	$\Delta G^{\ddagger}$	4.95	5.47	7.28	3.03	13.00[b]
	k_{rel}	1	1	1	1	1
2	$\Delta E^{\ddagger}$	3.92	4.93	6.78	3.24	
	$\Delta H^{\ddagger}$	3.87	4.89	6.77	3.13	13.21
	$\Delta G^{\ddagger}$	3.86	4.85	6.67	3.24	13.24[b]
	k_{rel}	6.3	2.9	2.8	0.7	0.7
3	$\Delta E^{\ddagger}$	2.88	4.05	5.74	2.27	
	$\Delta H^{\ddagger}$	2.85	4.01	5.73	2.17	12.37
	$\Delta G^{\ddagger}$	2.79	3.96	5.61	2.25	12.60[b]
	k_{rel}	38	13	17	3.7	2.0

[a] Results in kcal/mol from gas-phase geometry optimizations. $\Delta E^{\ddagger}$ (0 K) includes the zero-point energy change. $\Delta H^{\ddagger}$ and $\Delta G^{\ddagger}$ also include the thermal corrections to 298 K. Energies in kcal/mol. [b] From gas-phase FEP calculations.

Table 4. Free Energies of Activation ($\Delta G^{\ddagger}$ in kcal/mol) and Relative Rates in Aqueous Solution at 298 K

	HF-PCM/6-31+G(d,p)	MP2-PCM/6-31+G(d,p)	PDDG-PM3/MC/FEP	expt[a]
1	9.88	10.84	13.45	
2	7.63	8.44	11.43	
3	5.91	6.67	9.51	
k_{rel}**1**:**2**:**3**	1:45:810	1:5.8:1100	1:30:773	1:21:252

[a] References 8, 9.

Therefore, the $\Delta G^{\ddagger}$ values calculated for the cyclizations from QM/MM simulations were adjusted to include contributions from ΔG_{eq}. $\Delta G^{\ddagger}$ values computed in the gas phase and with continuum solvation were left unchanged (Tables 3 and 4).

For the gas phase, the results in Table 3 confirm that increasing methylation on C_1 generally leads to lower activation barriers and an increase of the reaction rate; however, the differential effects are small. The MP2 results indicate rate ratios of ca. 1:3:15 for **1**−**3**, while the higher-level CBS-Q calculations give 1:1:4, and PDDG/PM3 is in concurrence at 1:1:2. At the CBS-Q level, the activation barriers are all small at 2−3 kcal/mol, so the gas-phase reactions are very fast and affected little by the differences in methylation. The barriers from the PDDG/PM3 calculations are ca. 10 kcal/mol too high, though they mirror the trends from the MP2 and CBS-Q methods.

The results in Table 4 incorporate the effects of hydration. Hydration is predicted to increase the free energy barriers for calculations employing continuum solvation, while the MC/FEP protocol suggests the opposite trend. This will be discussed in more detail in the next section. However, the net outcome is the same, with decreasing free energy barriers in aqueous solution with increasing methylation. The implicit and explicit solvent models all yield an increase in the relative rate ratios for **1**−**3** as the differences between the energy barriers become larger. The computed rate ratios are now in much better accord with the observed rate data, and it is apparent that the dominant contributor to the *gem*-dimethyl effect for **1**−**3** is differential solvation. The likely explanation, considered further below, is that increasing methylation at C_1 interferes with hydrogen-bonding to the alkoxide oxygen, making it progressively more reactive.

It is noted that a potential complication in the comparison of computed and experimental rate ratios arises from possible contribution of the proton-transfer step in Scheme 1. If the proton transfer is not spontaneous ($K < 1$), the overall reaction rate would reflect the product of the equilibrium constant K for formation of the chloroalkoxide ion and the rate constant for the cyclization. The pK_a values for water and ethanol in aqueous solution at 25 °C are 15.7 and 15.9;[43] however, the pK_a for 2-chloroethanol (**1**) is 1.6 units lower, at 14.3, in view of the inductive effect of the chlorine.[43b] The pK_a values of 2-propanol and 2-methyl-2-propanol are less certain, but values of 16−17 and 16−19 are commonly quoted, respectively.[43] Recent textbooks are split between reporting 18.0 and 19.2 for the pK_a for 2-methyl-2-propanol without citation. The 19.2 value was derived from competition kinetics for reactions of hydroxide and alkoxide ions with 2,4-dinitrofluorobenzene.[43c] Applying the 1.6 unit offset for chlorination, the expected pK_a values for the alcohols **1**−**3** are roughly 14, 14−15, and 14−17. Thus, the proton transfer should be spontaneous for **1** and **2**, while it may contribute a little retardation to the observed rate of oxirane

(43) (a) Takahashi, S.; Cohen, L. A.; Miller, H. K.; Peake, E. G. *J. Org. Chem.* **1971**, *36*, 1205–1209. (b) Ballinger, P.; Long, F. A. *J. Am. Chem. Soc.* **1960**, *82*, 795–798. (c) Murto, J. *Acta Chem. Scand.* **1964**, *18*, 1043–1053.

Table 5. Calculated Geometrical Parameters for the Reactants and Transition Structures in the Gas Phase[a]

	bond angle or length	HF/6-31+G(d,p)	MP2/6-31+G(d,p)	MP2/6-311+G(d,p)	CBS-Q	PDDG/PM3
1	$\angle O-C_1-C_2$	107.9	107.6	108.5	106.0	109.9
2	$\angle O-C_1-C_2$	105.6	105.4	106.4	104.3	109.5
3	$\angle O-C_1-C_2$	103.3	103.2	104.2	102.6	108.4
1-TS	$\angle O-C_1-C_2$	91.0	87.8	86.8	89.8	86.3
2-TS	$\angle O-C_1-C_2$	90.9	87.3	86.3	89.5	86.5
3-TS	$\angle O-C_1-C_2$	90.7	87.0	85.9	89.6	86.9
1	$r(C_2-Cl)$	1.87	1.85	1.84	1.86	1.81
2	$r(C_2-Cl)$	1.88	1.85	1.84	1.87	1.81
3	$r(C_2-Cl)$	1.89	1.86	1.85	1.88	1.81
1-TS	$r(C_2-Cl)$	2.26	2.22	2.23	2.15	2.19
2-TS	$r(C_2-Cl)$	2.24	2.22	2.23	2.15	2.20
3-TS	$r(C_2-Cl)$	2.22	2.21	2.23	2.14	2.22

[a] Angles in degrees; bond lengths in Å.

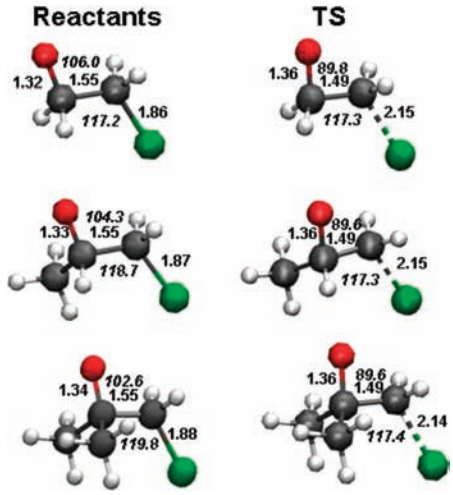

Figure 2. Optimized structures for the reactants and transition structures for **1**, **2**, and **3** (top to bottom) with CBS-Q in the gas phase. Key bond lengths (Å) are shown in bold; bond angles (°) are in italics.

formation for **3**. In turn, this may account for the larger computed k_{rel} values for **3** in Table 4 compared to the observed value.

Consistent with the Thorpe−Ingold hypothesis, the gas-phase structural results in Table 5 and Figure 2 do show that increased methylation on C_1 is accompanied by compression of the $O-C_1-C_2$ angle by 3−4° on going from **1** to **3**. However, the small angular variations have little energetic significance (Table 3).[13] In general, the structural results from the five QM methods are very similar. The CBS-Q structures for the transition states of **1**−**3** have slightly wider OCC angles (90°) and shorter C−Cl distances (2.15 Å) than in the MP2 and PDDG/PM3 results. So, the CBS-Q transition states are a little earlier along the reaction path than the others and yield lower activation barriers (Table 3).

Solvent Effects. Protic solvents usually retard the rates of intermolecular S_N2 reactions with anionic nucleophiles by stabilization of the charge-localized nucleophile through hydrogen-bonding more so than the more charge-delocalized transition state.[17,31,44] Although the results from calculations using continuum solvation are indicative of such a trend, the MC/FEP results show a general decrease in the activation barriers in solution compared to those in the gas phase. However, the net effect of increased reactivity with increasing methylation in both cases can be explained by steric hindrance to hydration of the nucleophilic oxygen by the methyl substituent(s) on C_1 in the reactants. In the continuum models, the absolute barriers increase owing to perceived better hydration of the reactants than transition states; however, the effect diminishes with increasing methylation owing to the reduction in exposed surface area for the nucleophilic oxygen. In the MC/FEP case, the free energy barrier does increase by 0.45 kcal/mol for **1** on going from the gas phase to aqueous solution (Tables 3 and 4). The decreases in the barriers for **2** and **3** can then again be attributed to progressively poorer hydration of the nucleophile. This is reflected in several ways, as shown in the following.

First, typical snapshots of the reactants and the transition structures from the MC/FEP simulations are provided in Figure 3. For the reactants, there is a cluster of 4−5 water molecules hydrogen-bonded to the oxygen atom, and there are 1−2 less tightly coordinated water molecules near the chlorine. For the transition structures, 4 water molecules remain hydrogen-bonded to the oxygen, and there are now an additional 4 water molecules associating with the chlorine, as it has gained significant partial negative charge. The snapshots suggest that, for the reactants, interactions with water are more favorable for **1**, showing an additional hydrogen bond, than for **2** or **3**. In turn, **2** has on average shorter and, thus, stronger hydrogen bonds than **3**. In comparing the reactants for **1** and **3**, it is clear that the water cluster on the oxygen is displaced away from the added methyl groups. The solvation of the transition structures for **1**−**3** seems more similar, with four water molecules clustered around both the oxygen and chlorine atoms. Overall, it appears that poorer hydration of the reactants with increasing methylation is the dominant effect.

The trends are better quantified by analyzing the solute−solvent energy pair distributions in two representative FEP windows, near the reactants and near the transition state (Figure 4). These results are averaged over the entire simulations. The distributions record the average number of water molecules that interact with the reacting system and their corresponding energies. Hydrogen bonds between the solute and water molecules are reflected in the left-most regions, with energies lower than ca. −5 kcal/mol. The large band near 0 kcal/mol arises from the many distant water molecules in the bulk. For the reactants, there is a single low-energy band reflecting the hydrogen bonds to the oxygen atom. It gradually shifts to higher energy with increasing methylation. Integration of the reactants' distributions from −20 kcal/mol to the minimum near −10 kcal/mol yields 4.6, 4.5, and 3.9 strongly hydrogen-bonded water molecules for **1**, **2**,

(44) Young-Ho, O.; Doo-Sik, A.; Sang-Yoon, C.; Jeong-Hwan, J.; Sung-Woo, P.; Seung, J. O.; Dong, W. K.; Hee, S. K.; Dae, Y. C.; Sungyul, L. *J. Phys. Chem. A* **2007**, *111*, 10152–10161.

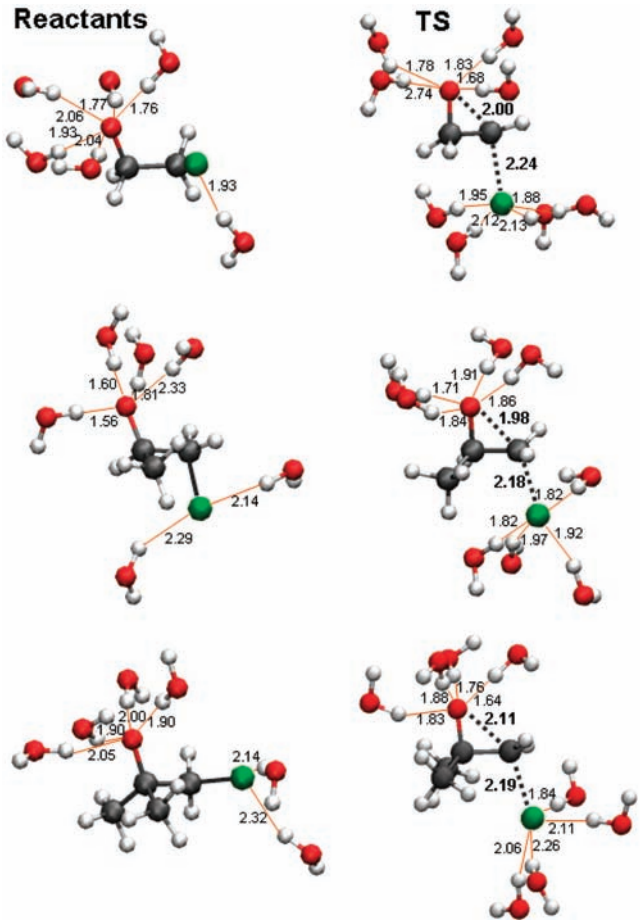

Figure 3. Typical snapshots of the reactants and the transition structures for **1**−**3** in water (only the nearest water molecules are illustrated) from the MC/FEP simulations. All distances are in Å.

and **3**, respectively, which is consistent with the snapshots in Figure 3. The shoulders centered near −7 kcal/mol likely reflect the weaker interactions with the chlorine atom in the reactants. At the transition state, the two features grow closer in energy, as negative charge has transferred from the oxygen to the chlorine atom. The diminished negative charge on oxygen causes its hydrogen-bonding band to shift its center to near −14 kcal/mol, while the hydrogen bonds to the chlorine atoms are reflected in the bands centered near −11 kcal/mol. Integration to the minima near −7 kcal/mol yields totals of 8.4, 7.2, and 7.7 hydrogen bonds for the transition states for **1**, **2**, and **3**, respectively, which is again consistent with Figure 3. The breakdown between hydrogen bonds to the oxygen and chlorine atoms is less certain owing to the overlap of the bands near −12 kcal/mol. However, integration from −20 kcal/mol to this point yields 3.7, 3.4, and 3.0 hydrogen bonds to the oxygen atom in the transition states for **1**, **2**, and **3**. Overall, the energy pair distributions show that there are 4−5 strong hydrogen bonds for the reactants that evolve to 7−8 weaker hydrogen bonds for the transition states. It is also clear that hydrogen-bonding to the reactant diminishes on progressing from **1** to the more hindered **3**.

The full impact of the hydrogen-bonding can be assessed by integrating the energy pair distributions, i.e., summing the populations multiplied by the interaction energies. The results are given in Table 6 for integration from −20 to −5 kcal/mol. This shows that the total interaction energy becomes less favorable by 20 kcal/mol with increasing substitution for the

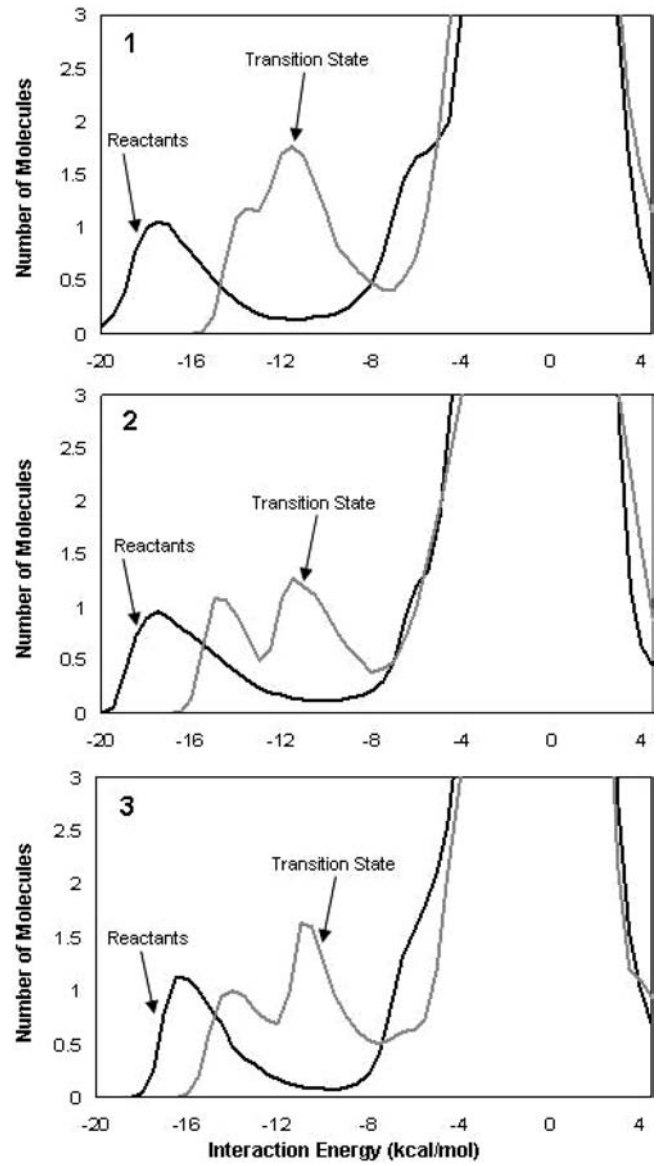

Figure 4. Solute−solvent energy pair distribution functions for the cyclization reaction of **1**, **2**, and **3** (top to bottom) for structures near the reactants and the transition states at 25 °C. The ordinate records the number of water molecules that interact with the solutes, with their interaction energy on the abscissa. Units for the ordinate are number of water molecules per kcal/mol.

Table 6. Number of Solute−Solvent Interactions, *N*, and Sum of Their Interaction Energies (kcal/mol)[a]

	N		ΣE_i	
	reactants	TS	reactants	TS
1	9.5	10.5	−106.0	−106.4
2	7.8	9.7	−91.7	−98.3
3	8.2	9.3	−85.2	−95.6

[a] From integrating the energy pair distributions (Figure 4) from −20 to −5 kcal/mol.

reactants **1**−**3**. The decline is only half this amount for the transition states. The pattern is fully consistent with the MC/FEP results in Table 4, which show the activation barriers decreasing with increasing substitution. The similar barriers in the gas phase (Table 3) and in aqueous solution (Table 4) for **1** from the PDDG/PM3-based calculations are also consistent with the essentially identical interactions energies (−106 kcal/

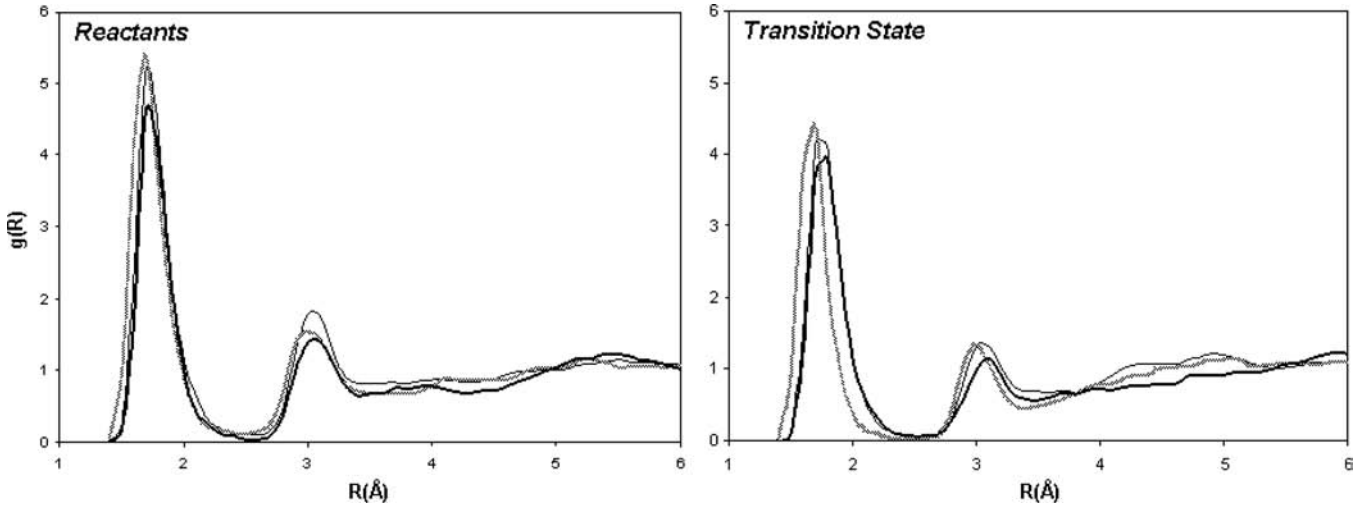

Figure 5. Computed O(solute)−H(water) radial distribution functions for the epoxidation reactions of 2-chloroethoxide analogues near reactants and the transition state: **1** (solid thin black curve), **2** (solid gray curve), and **3** (solid thick black curve) at 25 °C.

mol) in Table 6. The MC/FEP results state that the increased rates on going from **1** to **3** stem primarily from steric hindrance to hydration, having a greater effect on the reactants than on the transition states.

The present analysis is also confirmed by the computed solute−water radial distribution functions (rdf's). For example, the O−H rdf's, $g_{OH}(R)$, in Figure 5 give the normalized probability of occurrence of a water hydrogen a distance R from the oxygen atom of the solute. Hydrogen-bonding is reflected in the sharp first peaks, which extend to ca. 2.5 Å. There are two key observations: (a) for the reactants and transition states, the first peaks diminish and shift to larger R on progressing from **1** to **3**, and (b) there is less hydrogen-bonding to the nucleophilic oxygen atom in the transition states than in the reactants. For the reactants, integration of the first peaks to the minima near 2.5 Å reveals averages of 4.7, 4.6, and 4.0 hydrogen bonds between the solute's oxygen and water molecules for **1**, **2**, and **3**, respectively. For the transition states, the corresponding integrations yield 4.0, 3.2, and 3.8 hydrogen bonds. These values are similar to those from the energy pair distributions. The Cl−H rdf's (not shown) reveal the expected reciprocal pattern, with substantial strengthening of the first peak on going from the reactants to transition states.

The partial atomic charges for the reactants and transition states may also be noted (Table 7). The values shown are for the last configurations in the MC simulations, which are representative. As already known, hydrogen-bonding is sensitive to small charge shifts.[44−48] The principal expected pattern is apparent, with the negative charge declining on the oxygen atom and increasing on the chlorine atom on going from reactants to transition states. However, this charge change for the nucleophilic oxygen is relatively small (0.05−0.1 e), while the gain of negative charge on the chlorine atom (0.4 e) is pronounced. This is consistent with the substantial maintenance of hydrogen-bonding to the oxygen atom and large gain in hydrogen-bonding for the chlorine atom on progressing to the transition states (Figures 3 and 4). The small loss of negative charge on the oxygen still weakens the hydrogen bonds (Figure 4). The increase in positive charge on C_1 for the reactants with increasing methylation also weakens the hydrogen bonds, owing to increased repulsion with the hydrogen-bond-donating hydrogen atom of the water molecules.

Table 7. Computed CM3 Atomic Charges for the Reactants and Transition States[a]

		C_1	O	C_2	Cl
1	reactants	0.105	−0.868	−0.056	−0.326
	TS	0.025	−0.761	0.208	−0.788
2	reactants	0.141	−0.873	−0.032	−0.372
	TS	0.079	−0.757	0.179	−0.760
3	reactants	0.332	−0.823	−0.072	−0.324
	TS	0.243	−0.778	0.188	−0.712

[a] From the last configuration in the MC/FEP calculations in water at 25 °C.

Finally, before closing, additional experimental data may be mentioned for analogues of **1**−**3** with methylation at C_2. For the series $HOCH_2CH_2Cl$ (**1**), $HOCH_2CH(CH_3)Cl$ (**4**), $HOCH_2C(CH_3)_2Cl$ (**5**), the relative reaction rates in water with NaOH as base are 1:5.5:248.[8,9] On the basis of the present results, the lowest energy conformer for the corresponding alkoxide ions can be expected to be *anti* in each case. The small rate difference between **1** and **4** then reflects little difference in intrinsic reactivity and in steric hindrance to hydration of the nucleophilic oxygen atom. For **5**, the presence of the two methyl groups *gauche* to the oxygen atom may provide some shielding of the nucleophile, and since the chloride is now tertiary, greater C^+-Cl^- charge separation can be expected in the transition state, along with stronger hydrogen-bonding to the leaving group. Further investigation of these systems, especially with gas-phase experiments, would be valuable.

Conclusions

Quantum and statistical mechanics calculations were carried out for the base-initiated cyclization reactions of **1**− **3** in order to investigate the experimentally observed rate enhancements in aqueous solution resulting from increased methylation on C_1. Traditionally, the acceleration has been attributed to the Thorpe−Ingold effect, whereby increased methylation decreases

(45) Chandrasekhar, J.; Shariffskul, S.; Jorgensen, W. L. *J. Phys. Chem. B* **2002**, *106*, 8078–8085.
(46) Blake, J. F.; Jorgensen, W. L. *J. Am. Chem. Soc.* **1991**, *113*, 7430–7432.
(47) Blake, J. F.; Lim, D.; Jorgensen, W. L. *J. Org. Chem.* **1994**, *59*, 803–805.
(48) Jorgensen, W. L.; Blake, J. F.; Lim, D.; Severance, D. L. *Trans. Faraday Soc.* **1994**, *90*, 1727–1732.

the backbone CCC angle between the reacting partners. However, gas-phase quantum mechanical calculations at the MP2 and CBS-Q levels showed that there is little difference in intrinsic reactivity for **1**− **3** (Table 3). Subsequent consideration of continuum hydration or MC/FEP calculations in explicit water reproduced well the observed reactivity pattern (Table 4). Thus, the Thorpe−Ingold acceleration for **1**−**3** is primarily a solvent effect. The MC/FEP calculations also allowed thorough analysis of the origins of the rate variations through analysis of hydrogen-bonded structures, solute−water energy pair distributions, and radial distribution functions (Figures 3−5). This provided consistent evidence that the principal origin of the rate enhancement on going from **1** to **3** arises from increased steric hindrance to hydration of the nucleophilic oxygen atom with increasing α-methylation. Though there has been great interest in Thorpe−Ingold and *gem*-disubstituent effects, the potential role of solvent effects in the kinetics of the investigated reactions has not previously received significant attention.[8] Hopefully, the present study will stimulate further efforts that are essential to yield deeper understanding of the true origins of rate variations and catalytic effects.

Acknowledgment. Gratitude is expressed to the National Science Foundation and National Institutes of Health (GM32136) for support of this work, to Prof. Dale L. Boger for discussions, and to Dr. Julian Tirado-Rives for multifaceted assistance.

Supporting Information Available: Full citation for ref 42; tables of total gas-phase energies, enthalpies, and free energies for the reactants and transition states from the quantum mechanical calculations; and Cartesian coordinates for the reactants and transition states from the CBS-Q calculations. This material is available free of charge via the Internet at http://pubs.acs.org.

JA1023755